NEUROSCIENCE
RESEARCH ARTICLE

INTERNATIONAL BRAIN IBRO RESEARCH ORGANIZATION

J. Kaiser et al. / Neuroscience xxx (2021) xxx–xxx

Emulating Dendritic Computing Paradigms On Analog Neuromorphic Hardware

Jakob Kaiser,[a] Sebastian Billaudelle,[a] Eric Müller,[a] Christian Tetzlaff,[b] Johannes Schemmel[a] and Sebastian Schmitt[b]*

[a] *Heidelberg University, Kirchhoff-Institute for Physics, Germany*

[b] *University of Göttingen, Third Institute of Physics, Germany*

Abstract—BrainScaleS-2 is an accelerated and highly configurable neuromorphic system with physical models of neurons and synapses. Beyond networks of spiking point neurons, it allows for the implementation of user-defined neuron morphologies. Both passive propagation of electric signals between compartments as well as dendritic spikes and plateau potentials can be emulated. In this paper, three multi-compartment neuron morphologies are chosen to demonstrate passive propagation of postsynaptic potentials, spatio-temporal coincidence detection of synaptic inputs in a dendritic branch, and the replication of the BAC burst firing mechanism found in layer 5 pyramidal neurons of the neocortex. © 2021 Published by Elsevier Ltd on behalf of IBRO.
This article is part of a Special Issue entitled: SI: Dendrites.

Key words: multi-compartmental models, accelerated technology, physical model, mixed-signal neuromorphic, AdEx neuron model.

INTRODUCTION

The dendritic structure equips neurons with the possibility to pre-process synaptic input before it is integrated at the soma (Koch and Segev, 2000; Euler et al., 2002; London and Häusser, 2005; Major et al., 2013). How this synaptic input is processed in the dendritic tree is influenced by a number of factors such as their morphology, ion channel distribution and the spatio-temporal distribution of the inputs themselves and therefore offers the possibility to perform a large set of different computations (Vetter et al., 2001; Schaefer et al., 2003; Williams and Stuart, 2002; Polsky et al., 2004).

For example, passive properties of dendrites can be utilized to enhance the coincidence detection of neurons and to enable direction selectivity at the single neuron level (Agmon-Snir et al., 1998; Tukker et al., 2004). Furthermore, active channels allow dendrites to pre-process synaptic input locally in form of dendritic spikes (Helmchen et al., 1999; Golding and Spruston, 1998; Schiller et al., 2000; Major et al., 2013).

Due to this local processing of inputs, multi-compartment neurons have been modeled as sets of computational subunits (Poirazi et al., 2003; Larkum et al., 2009; Ujfalussy et al., 2018); this approach is similar to multi-layered networks of point neurons and illustrates the computational power of multi-compartment neurons. Similarly, due to the possibility to integrate feed-forward and feedback information independently, multi-compartmental neuron models have also been used in the quest to solve the credit assignment problem (Urbanczik and Senn, 2014; Guerguiev et al., 2017; Sacramento et al., 2018; Richards and Lillicrap, 2019).

The dendritic structure also offers new possibilities in the formulation of learning algorithms. Dendritic spikes can be used to trigger plasticity locally without the need of an axonal action potential (Golding et al., 2002). The spatial extent of dendrites can also be used to employ different learning rules at different locations within the same neuron (Bono et al., 2017).

Naturally, researchers aim to exploit the computational power of dendrites. Including non-linear dendrites and structured neurons in simulations is computationally costly and limits the selection of available simulators (Carnevale and Hines, 2006; Akar et al., 2019; Stimberg et al., 2019). Analog neuromorphic computing offers an alternative. It replaces the numerical calculations with an emulation of the temporal dynamics of biological neurons using micro-electronic technology. Voltages and currents of the model are represented directly by corresponding values in the electronic circuits. Emulation is time-continuous and follows the dynamics of the underlying differential equations.

Several attempts to include dendritic computation in neuromorphic implementations have been reported (Wang and Liu, 2011; Ramakrishnan et al., 2013; Kousanakis et al., 2017; Bhaduri et al., 2018). The detail level of these implementations varies from representing a structured neuron by a two-layer network of non-linear

*Corresponding author.
E-mail address: sebastian.schmitt@phys.uni-goettingen.de (S. Schmitt).

https://doi.org/10.1016/j.neuroscience.2021.08.013
0306-4522/

units (Kousanakis et al., 2017; Bhaduri et al., 2018) to implementing 2D arrays of dendritic compartments which allow to emulate custom neuron morphologies (Wang and Liu, 2011; Ramakrishnan et al., 2013). The BrainScaleS-2 (BSS-2) system falls in the second category and allows to emulate various biologically realistic neuron morphologies.

The implementations presented in Wang and Liu (2011), Ramakrishnan et al. (2013), and Bhaduri et al. (2018) operate in biological real-time and use the sub-threshold operation mode of the transistors. With the exception of Ramakrishnan et al. (2013), none of them include hardware support for long and short-term plasticity of weights, topology and neuron physiology. The neuromorphic system discussed in this paper, BSS-2, has been designed as an emulation platform for neuroscientific research and differs from previous implementations in several aspects.

First, it support the calibration of the neurons physiological parameters, like multiple synaptic time constants, different reversal potentials and inter-compartmental conductances to allow a faithful representation of the biological model by using a digitally controlled local analog parameter storage with 24 individual parameters for each dendritic compartment (Hock et al., 2013). Individual calibration is also supported in Ramakrishnan et al. (2013) by the means of floating-gate technology. Second, it operates at an acceleration factor of 1000, i.e. all time-constants are 1000 times shorter compared to biology. This allows to use it for high-dimensional parameter searches, hyperparameter optimization and the investigation of learning rules on a long timescale. Third, it has build-in support for structural plasticity to emulate a wide range of developmental and learning processes. Regarding dendritic computation, it is able to emulate a wide range of neuron morphologies, bidirectional signal propagation in dendrites and the generation of dendritic spikes.

All experiments presented in this paper are executed on the latest version of the BSS-2 system. Previous revisions and smaller-scale prototype versions have already been used to perform a variety of experiments (Aamir et al., 2018; Göltz et al., 2019; Cramer et al., 2020; Billaudelle et al., 2020; Billaudelle et al., 2021; Cramer et al., 2020). After giving an overview of the hardware implementation and its configuration space, we show three experiments which showcase the passive propagation of electric signals, the generation of dendritic spikes and the interplay of different compartments of a structured neuron.

EXPERIMENTAL PROCEDURES

BSS-2 is a mixed-signal, neuromorphic chip implemented in a 65nm CMOS technology. Neurons and synapses are implemented by analog circuits operating in continuous time. Compared to the biological archetype, circuit dynamics typically evolve 1000 times faster. Communication of spike events and configuration data is handled by digital logic[1] (Schemmel et al., 2017; Aamir et al., 2018a; Aamir et al., 2018b).

Neuron circuit

512 analog neuron circuits on the chip implement the dynamics of the adaptive exponential integrate and fire (AdEx) neuron model (Brette and Gerstner, 2005) with the possibility to connect multiple circuits to emulate multi-compartmental neurons. Each compartment aims to replicate the following dynamics of the membrane voltage $V_\mathrm{m}(t)$:

$$\begin{aligned} C_\mathrm{m}\frac{\mathrm{d}V_\mathrm{m}(t)}{\mathrm{d}t} &= g_\mathrm{leak}\cdot(V_\mathrm{leak}-V_\mathrm{m}(t)) \\ &+ g_\mathrm{leak}\Delta_\mathrm{exp}\exp\left(\frac{V_\mathrm{m}(t)-V_\mathrm{exp}}{\Delta_\mathrm{exp}}\right) \\ &+ I_\mathrm{syn}(t) - w(t) + I_\mathrm{MC}(t), \end{aligned} \tag{1}$$

where C_m is the membrane capacitance, g_leak the leak conductance, V_leak the leak potential, Δ_exp the exponential slope factor and V_exp the exponential threshold. The synaptic current $I_\mathrm{syn}(t)$ is modeled by current-based synapses with an exponentially decaying kernel.

$w(t)$ represents an adaptation current with the following dynamics

$$\tau_\mathrm{w}\frac{\mathrm{d}w(t)}{\mathrm{d}t} = a(V_\mathrm{m}(t)-V_\mathrm{leak}) - w(t), \tag{2}$$

with an adaptation time constant τ_w and a scaling factor a. Whenever the neuron spikes w is incremented: $w \to w + b$ (Aamir et al., 2018a).

I_MC denotes the current originating from connected compartments and is given by the sum over all connected compartments j:

$$I_\mathrm{MC}(t) = \sum_j g_j\cdot\left(V_\mathrm{j}(t)-V_\mathrm{m}(t)\right). \tag{3}$$

g_j represents the conductance between the considered compartment and the neighboring compartment j while $V_j(t)$ is the membrane voltage of this neighboring compartment.

Once the membrane voltage V_m reaches the threshold voltage V_th a digital spike event is generated and the membrane is reset via a conductance-based reset: the membrane connects to the reset potential V_reset via a conductance g_reset for the duration of the refractory period τ_ref, Fig. 2. After the refractory period the evolution of V_m is again given by Eq. 1.

The silicon neuron circuits of BSS-2 are designed for a membrane time constant $\tau_\mathrm{m} = C_\mathrm{m}/g_\mathrm{leak}$ which is 1000 times smaller than in biological neurons. As a result the dynamics evolve with time constants in the microsecond regime rather than in the millisecond regime as in biology. Throughout this paper times and voltages will be given in the hardware domain if not stated explicitly otherwise.

The neuron circuit design offers a high degree of configurability and all variables introduced in Eq. (1) can

[1] Off-chip I/O uses 8-Gbit/s highspeed links providing a reliable transport layer for configuration data and low-latency transfer of events. For off-chip communication, spike events contain a timestamp and a label encoding source or target information. Compared to configuration data they are prioritized. For more information see Schemmel et al. (2020).

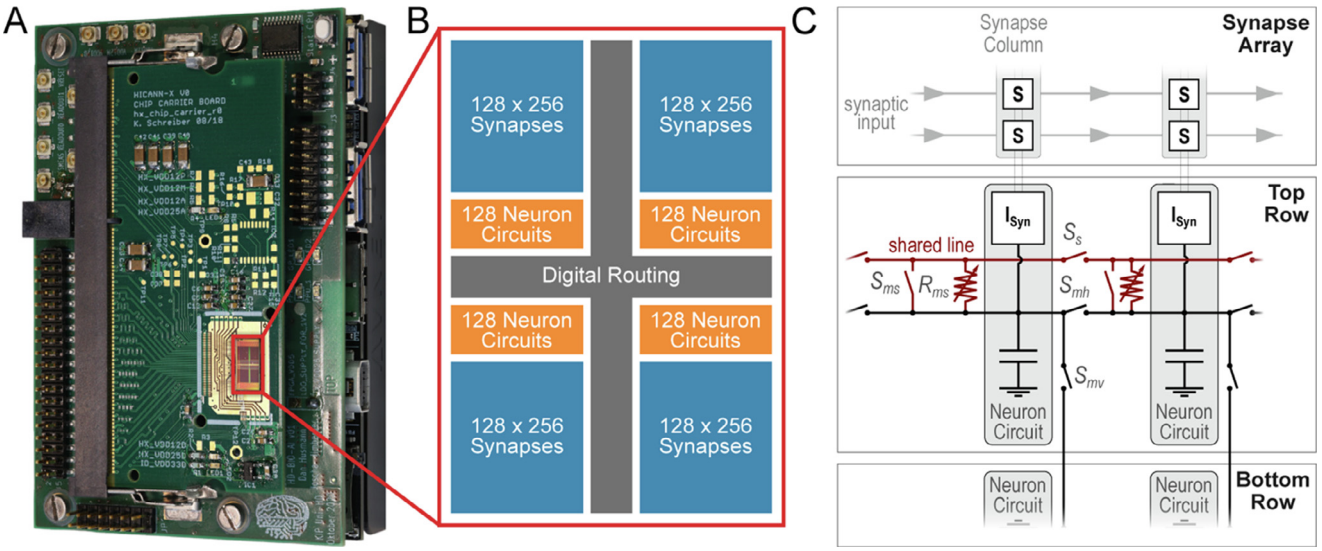

Fig. 1. System overview: (**A**) BSS-2 mobile system. The neuromorphic chip is bonded to a carrier board which is connected to a FPGA and a CPU performing experiment control and providing an interface to the system. (**B**) Schematic of the BSS-2 neuromorphic chip. The chip is divided in 4 quadrants. Each quadrant is equipped with 128 analog neuron circuits and 32768 analog synapses. Spike events are handled by digital logic. (**C**) Each neuron circuit is represented by a capacitor and the synaptic input; other parts, for example, spiking threshold or adaptation are not displayed, see Aamir et al. (2018). Each circuit receives synaptic input from one synapse column and integrates it on its membrane. Larger logical neurons can be formed by connecting several circuits by closing the transmission gate switches in the horizontal S_{mh} or vertical S_{mv} direction. The horizontal switch allows to connect neighboring neurons in the same quadrant, while the vertical switch allows to connect neurons in different neuron rows (in subfigure B the rows are separated by the digital routing). In addition a shared line can be used to connect different neuron circuits. In contrast to the "direct" connection via the membrane switches, this allows to place resistors between different neuron circuits and therefore for the formation of multi-compartment neurons. Each neuron circuit can connect to this shared line via a switch S_{ms} or via a tunable conductance R_{ms}. Fig. 3 shows how this can be used to form structured neurons. Subfigure C is adapted from Aamir et al. (2018).

be configured independently for each instance of the neuron circuit.

On BSS-2 spikes are represented by packets containing labels. These labels are used at several locations on the chip to decide how events are forwarded and therefore allow for the implementation of flexible network topologies. To establish a connection between two neurons, spikes are routed from the pre-synaptic neuron to the synapse drivers at the edge of the synapse array, Fig. 1B. The synapse drivers forward these events to rows of synapses and at each synapse a locally stored label is compared to the label in the spike package. If the labels match the signal is scaled by a locally stored six bit weight and forwarded to the post-synaptic neuron which is at the end of the synapse column, compare Fig. 1B and C.

With this configuration each neuron circuit can receive inputs from a column of 256 current-based synapses. Switches S_{mv}/S_{mh} between neighboring neuron circuits allow the circuits to be connect, increasing the fan-in of single logical neurons, Fig. 1C. The total number of logical neurons can therefore be traded for a higher fan-in of individual neurons. The configuration of the switches as well as other digital neuron parameters are stored in local static random-access memory (SRAM).

Dendritic spikes

Supra-linear summation of synaptic input in form of dendritic spikes can increase the computational power of dendrites (Poirazi and Mel, 2001; London and Häusser, 2005). The BSS-2 system can replicate this non-linear response.

Each compartment itself consists of a fully functional neuron circuit, see next section, and sodium-like spikes are easily modeled by the AdEx model implementation, Fig. 2A. Dendritic plateau potentials can be reproduced by utilizing the conductance-based reset to pull the membrane voltage V_m above the threshold voltage V_{th}, Fig. 2C. This is achieved by setting the reset voltage V_{reset} above the threshold voltage V_{th}.

The reset potential V_{reset} and conductance g_{reset} can be set individually for each neuron circuit such that different compartments can have different spiking behavior. Furthermore, the refractory times τ_{ref} can be set in a range from the sub-microsecond to the millisecond regime and therefore allow for a large range of plateau potential durations.

Structured neuron

In addition to the low-ohmic connections S_{mv}/S_{mh}, neuron circuits can also be connected via adjustable conductances. For that purpose a shared line runs at the top of the neuron circuits, Fig. 1C. Each neuron circuit can connect to this shared line either via a switch S_{ms} or via an adjustable conductance R_{ms}. The connectivity of the shared line can be controlled by switches S_s between neuron circuits. By closing the switches and therefore connecting the shared lines, complex multi-compartment models can be implemented on BSS-2.

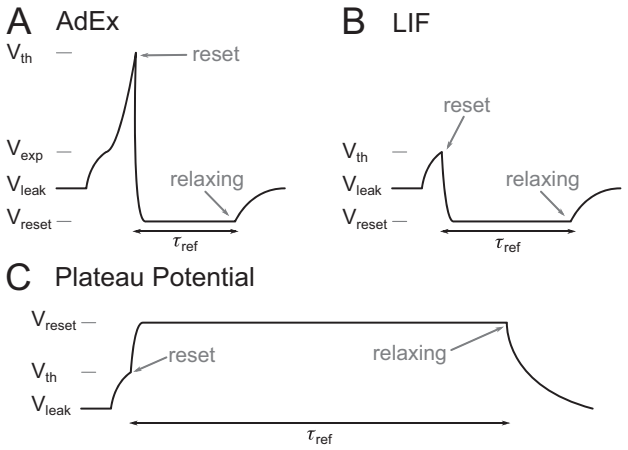

Fig. 2. Spiking behavior on BSS-2. The subfigures sketch how the membrane voltage $V_m(t)$ responses in different spike modi. (**A**) Response in AdEx mode. Once the exponential threshold V_{exp} is reached the membrane voltage increases rapidly until the threshold V_{th} is hit. At this point the conductance based reset is triggered: the membrane is connected to the reset voltage V_{reset} via a high conductance g_{leak}. After the refractory period τ_{ref} ends the membrane voltage relaxes back to the leak potential V_{leak}. (**B**) In the LIF mode the exponential term is disabled. The membrane voltage is connected to the reset once the threshold voltage V_{th} is reached. Once again, the high conductance reset is used to pull the membrane potential below the leak potential $V_{threshold}$. **C** In order to generate plateau potentials the LIF mode is used and the reset voltage V_{reset} is set above the threshold voltage V_{th}. As a result the membrane voltage increases once the threshold is reached. After the refractory time, which is chosen to be longer than in the previous cases, the membrane relaxes back to the leak potential V_{leak}.

All 256 neuron circuits on one half of the chip can be connected in this fashion; due to the digital logic at the center of the chip the shared line can not be connected between the left and right half of the chip, Fig. 1B.

Fig. 3 illustrates how different multi-compartment models can be mapped on hardware. Simple two- and three-compartment models have for example been used to study the interaction between different spike initiation zones or learning algorithms (Larkum et al., 2001; Larkum et al., 2004; Urbanczik and Senn, 2014; Guerguiev et al., 2017; Yi et al., 2017; Sacramento et al., 2018). These models can be mapped with a single neuron circuit per compartment, Fig. 3A and B.

Fig. 3B shows a three-compartment model which couples a somatic compartment (with sodium-spike dynamics) via an apical compartment to a tuft compartment with calcium-spike dynamics and its representation on hardware. The neuron circuits which represent the two different spike initiation zones connect via the adjustable conductances R_{ms} to the shared line while the apical compartment uses the low-ohmic connection S_{ms}; the switches S_s between the different compartments are closed to connect all three neuron circuits. The sodium dynamics in the somatic compartment can be replicated with the AdEx neuron model, while calcium-spikes are modeled by plateau potentials.

Listing 1 shows an example of how to configure this three-compartment model on hardware. Currently, multi-compartment neurons are formed by setting the switches and conductances, Fig. 1C, between different compartments explicitly in software. For point neurons the BSS-2 software infrastructure supports the PyNN language (Davison et al., 2009) to describe neural network models (Müller et al., 2020). We aim to include sup-

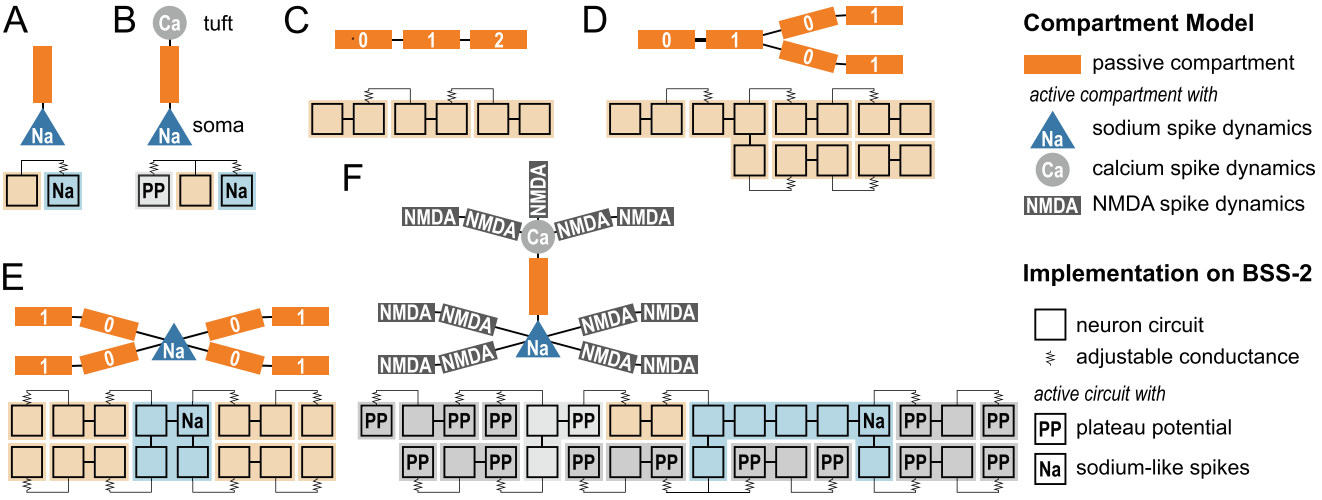

Fig. 3. Examples of multi-compartment neurons and their implementation on BSS-2. In each subfigure the compartmental model is at the top and the hardware implementation at the bottom. The diagrams of the hardware implementation are a simplification of Fig. 1C: each circuit is represented by a box and the vertical line as well as connection between neuron circuits are only displayed when connected. (**A**) Two-compartment model with one passive, dendritic compartment and a somatic compartment. (**B**) Three-compartment model with two spike initiation zones separated by a passive compartment. (**C**) Chain of compartment which could for example model a (long) dendritic branch. (**D**) Several chains can be combined to form a branching structure. This could replicate a thick dendrite which splits into to thinner branches. (**E**) A somatic compartment is connected to four dendritic branches with two compartments in each branch. **F** This multi-compartmental model of a pyramidal neuron is taken from Larkum et al. (2009) and shows how the previous elements can be combined to form more complex morphologies.

port for multi-compartment neurons in future versions of PyNN allowing for the easy definition of morphologies. This will allow non-expert users to perform experiments involving multi-compartment neurons on BSS-2.

```
# Modules:
#   - lola: bss2 chip configuration data
#   - halco: bss2 coordinate system

# Ca compartment
comp_ca = lola.AtomicNeuron()
comp_ca.multicompartment.enable_conductance = True
comp_ca.multicompartment.connect_soma_right = True

# Passive compartment
comp_pas = lola.AtomicNeuron()
comp_na.multicompartment.connect_soma = True
comp_na.multicompartment.connect_soma_right = True

# Na compartment
comp_na = lola.AtomicNeuron()
comp_na.multicompartment.enable_conductance = True

# ...
# Set other parameters of the neuron circuits
# ...

# Write configuration to hardware
for neuron_id, comp in enumerate([comp_ca, comp_pas, comp_na]):
    builder.write(halco.AtomicNeuronOnDLS(neuron_id), comp)
```

Listing 1: Configuration of a three-compartment neuron as displayed in fig. 3 B. Only the configuration of the dendritic structure is described and setting other parameters (compare eqs. (1) and (3)) is omitted. A neuron circuit on BSS-2 is represented by a `lola.AtomicNeuron`. We define the connections to the shared line before writing this configuration with the help of a configuration `builder` to hardware. The location at which a configuration is written is defined via a coordinate `halco.AtomicNeuronOnDLS` in the call to `builder.write` (Müller et al., 2020). We could add a constant offset to the variable `neuron_id` to place the configurations at a different location on the chip.

The next three examples, Fig. 3 C to E, provide building blocks to form a more complex model of a pyramidal neuron which was published by Larkum et al. (2009), Fig. 3 F.

A chain of compartments can be formed in a single row of neuron circuits, Fig. 3 C. Compartments in the middle of the chain have two neighboring compartments; therefore, they have to establish two connections to the shared line. This can only be achieved if each compartment is made up of at least two neuron circuits since the shared line has to be "interrupted" between these two connections, compare Fig. 1 C. The end compartments are also implemented with two circuits to emphasize that this structure can easily be extended to build longer chains.

These chains of compartments can be used to model a branching chain; this could for example represent a thick dendrite which splits into two thinner dendrites, Fig. 3 D. Both rows of neuron circuits are needed to replicate this structure on hardware: two chains are placed in the top row and connected in the same fashion as before; the last compartment of the first chain is extended with an additional neuron circuit on the bottom row, an additional chain is placed next to it and connected.

The high configurability of the BSS-2 system allows users to choose neuron properties such as capacity C_m and leak conductance g_{leak}, compare eq. 1, for each compartment separately; the conductance between compartments g_j, compare 3, can also be set individually. This, for example, allows for lower conductances between compartments of "thin" dendrites or lower capacitances for these compartments.

Similarly, we can model a somatic compartment which is connected to four dendritic branches, Fig. 3 E. This time the somatic compartment is represented by four neuron circuits; each circuit connects to a chain of compartments which model dendritic branches.

These basic structures can now be combined to implement a model of a pyramidal neuron as proposed by Larkum et al. (2009), Fig. 3 F. A somatic compartment is able to initiate sodium spikes and is connected to several basal dendrites. Via the apical trunk the soma is connected to a calcium spike initiation zone. This zone in turn is connected to several thin apical tuft dendrites. The basal and apical tuft dendrites themselves are modeled by up to two compartments which are capable of generating N-Methyl-D-Aspartat (NMDA) plateau potentials.

On hardware the basal dendrites and the somatic compartment are implemented similarly as in the example before but this time the somatic compartment extends in a U-shape over seven circuits to make place for one additional dendritic branch. This is necessary since the somatic compartment could otherwise not establish all five necessary connections. The circuits of the basal dendrites are configured to generate plateau potentials which emulate NMDA potentials. Two circuits are sufficient to model the apical dendrite which behaves purely passive in our example. The compartment with calcium-spike dynamics is once more configured to generate plateau potentials and spans over three circuits. In the upper row a part of the shared line is used to connect two different compartments at the same time, replicating the dendritic branch with one compartment and one of the branches with two compartments.

RESULTS

Passive properties

To illustrate the ability of the system to emulate the passive properties of dendrites, we consider a chain of compartments. In Fig. 3 C a chain of three compartments which are connected via fixed conductances is illustrated. As discussed in the previous section this model can easily be extended to longer chain lengths.

The leak voltages V_{leak} as well as time constants of the different compartments are calibrated to yield similar values.

In order to illustrate how excitatory post synaptic potential (EPSP) propagate along the chain of four compartments, we record the membrane traces[2] of all compartments while injecting a synaptic current in one of the compartments Fig. 4 A. The trace in the top left

[2] All membrane traces in this paper are recorded with an on-chip analog-to-digital converter (ADC). This ADC is used to record one trace at the time. As a consequence recordings from different compartments result from separate executions on hardware.

Please cite this article in press as: Kaiser J et al. Emulating Dendritic Computing Paradigms On Analog Neuromorphic Hardware. Neuroscience (2021), https://doi.org/10.1016/j.neuroscience.2021.08.013

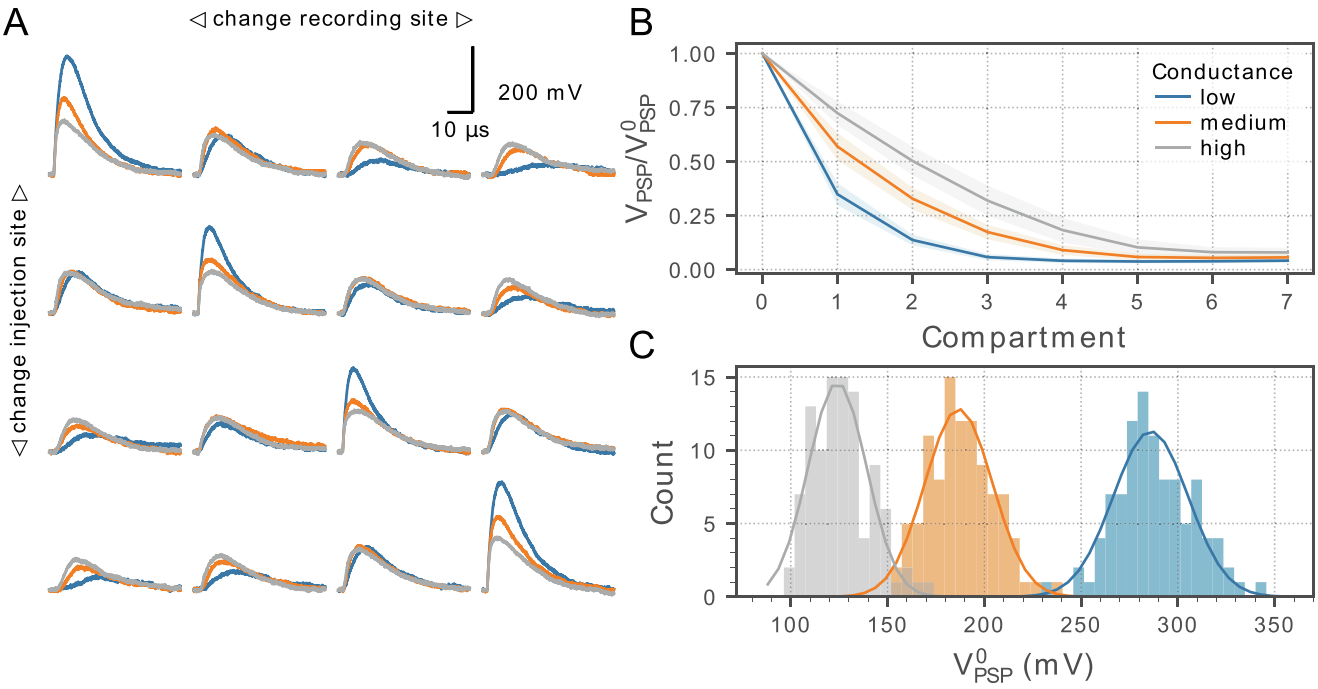

Fig. 4. Passive propagation along a chain of compartments emulated on BSS-2. (**A**) Membrane voltages of a chain with length four. For each compartment the membrane was recorded as an EPSP traveled along the chain. This was done for three different conductances. In the horizontal direction the recording compartment was changed, in the vertical direction the synaptic current was injected in different compartments. Given the same synaptic strength the height of the EPSP at the injection site increases with a decreasing conductance. The pulse height attenuates as the pulses travel along the chain. (**B**) Height of the EPSP V_{PSP} in the different compartments of an eight links long chain normalized to the EPSP height in the first compartment V^0_{PSP}. The attenuation was measured for three different conductances and 100 different placements on the chip. The solid lines represent the mean value averaged over all placements, the shaded area the standard deviation. As expected, the attenuation increases with an increasing resistance. (**C**) EPSP height in the first compartment for the same three conductances as before and a chain length of four. The histograms represent the heights for different placements on the chip. Due to the manufacturing process the height of EPSP varies from placement to placement. The mean EPSP height increases with increasing resistance, as seen in A. As the resistance increases the variance of the distributions increases as well; this is most evident when comparing the Gaussian fits. The spread of the distributions could be minimized by calibrating the conductances between different compartments and the synaptic weights.

shows the response in the first compartment to a synaptic input in the same compartment. As the conductance between the different compartments is increased the pulse height at the injection site decreases. This is expected since more current flows to the neighboring compartment.

Due to inherent properties of the manufacturing process, each neuron as well as each synaptic circuit behaves slightly differently. This is visible in Fig. 4C where the same digital weight values lead to different EPSP heights as the chain is placed at different locations on the chip. Several factors account for this variation, such as different strength in synaptic input and varying conductances between the compartments—the effect of these factor could be minimized by calibration. The mean of the EPSP height distribution shifts to smaller values and the standard deviation of the distribution decreases as the conductance is increased. A decrease in EPSP height for larger conductances was already evident in Fig. 4A.

As the pulses propagate along the chain their heights decrease. The attenuation of the pulse height V_{PSP} with respect to the height in the first compartment V^0_{PSP} is displayed in subfigure B for a chain of length eight. The attenuation was measured for 100 different placements on the chip; the solid line represents the mean attenuation while the colored area illustrates the standard deviation over different placements.

In cable theory the electronic length $\lambda = \sqrt{\frac{a \cdot r_m}{2 \cdot r_a}}$ is a measure for the spatial spread of electric perturbations (Rall, 1959). Here a describes the radius of the cable segment, r_m the radial resistance for unit area and r_a the axial resistance for unit length. On BSS-2 the resistance between neuron compartments, R_{ms} in Fig. 1C, can be used to control the attenuation of EPSP along the chain, Fig. 4B. While the pulse is almost extinguished in the fourth compartment for the lowest conductances displayed, the pulse has still more than a quarter of its original height for the high conductance. Similarly, the leak conductance g_{leak} can also be utilized to alter the spatial spread (data not shown).

Fig. 4A, second row, further shows that when a stimulus is injected to the second compartment the propagated pulse is higher in the compartment left to the injection site as compared to the compartment on the right. This is an effect of the finite chain length. As the compartment on the left is at the end of the chain it is only connected to one compartment and less current flows away from its membrane as compared to the compartment on the right which has two neighboring compartments. Similarly, the effect of a finite chain length can also be observed when considering the

EPSP height at different injection sites: the absolute height of the pulse injected in the second compartment is lower than the height of the pulse injected in the first compartment, comapre first and second row in Fig. 4A.

Dendritic coincidence detection

Dendrites can respond in a supra-linear fashion to synaptic input by generating dendritic spikes. This allows for local computations in dendrites and can have a pronounced effect on the somatic firing behavior (Golding and Spruston, 1998; Larkum et al., 1999; Larkum et al., 2004; Larkum et al., 2009; Yi et al., 2017). The integration of synaptic inputs in dendrites depends on their spatio-temporal distribution (Williams and Stuart, 2002; Polsky et al., 2004); the following experiments show how this behavior can be replicated on BSS-2.

We model a thick dendrite which merges into two thinner dendrites by a Y-shaped multi-compartment model, Fig. 5A. This arrangement is similar to the one presented in Fig. 3D but this time each branch is made up of four compartments; the implementation on hardware is easily realizable by repeating the two latest neuron circuits in each branch two times. Once again time constants as well as leak potentials are configured to yield similar values in all compartments; for conductances between compartments we use the "high" conductance of the previous experiment.

Compartment 0, blue in Fig. 5A, is configured to generate plateau potentials once a threshold voltage V_{th} is crossed. We now investigate which combination of synaptic inputs can elicit this dendritic plateau potential. Even though we do not look at the membrane traces in the hatched compartments we include them in our model since the morphology affects the electric properties of the neuron (Vetter et al., 2001; Schaefer et al., 2003); this effect was also seen in the first example, where EPSP tended to be higher at the end of the chain, compare Fig. 4A.

One synaptic input is always injected in *compartment 0*. An additional input is placed on the same or another compartment within the same branch, colored in Fig. 5A. This is done for different delays D between the two synaptic inputs.

Example recordings of the membrane voltage V_m in *compartment 0* are shown in Fig. 5B for different sites of the additional input. For the first trace both inputs were injected in *compartment 0* with a delay of 15 μs. The first input alone is not sufficient to reach firing threshold and the second input is needed to generate a dendritic plateau potential with a height of approximately 300 mV and a length of about 60 μs.

A synaptic current to a more distal compartment caused a slightly lower response on the membrane voltage as it gets attenuated during its propagation to the spike initiation zone. Nevertheless, the sum of both inputs is still high enough to cross threshold. For synaptic inputs which are injected even more distally the threshold can not be crossed in the displayed examples. Similarly, if the additional input is injected in *compartment 1* 15 μs before the input to *compartment 0*, no dendritic spike is triggered.

To further investigate which spatio-temporal spike combinations elicit a dendritic spike, we injected synaptic inputs in each compartment for delays between −50 μs to 50 μs in the different compartments. Each configuration was measured 200 times to gather statistics, Fig. 5D. The blue line indicates two inputs to *compartment 0*. As both inputs are chosen to have the same strength, the spiking probability is symmetrical around zero delay. For a broad range of around −15 μs to 15 μs a spike could be initiated in all trials. For larger differences between the incoming stimuli the spiking probability quickly drops to zero.

If the additional stimulus is injected more distally from the spike initiation zone the spiking probability becomes asymmetrical around zero delay and earlier distal inputs are preferred. While the probability for eliciting a spike already decreases to zero if the distal input is about 5 μs after the input to *compartment 0*, the probability stays at about one for delays up to around −10 μs.

As the input from *compartment 1* is attenuated the falling flank of its EPSP is less steep at the spike initiation zone as compared to the EPSP which is caused by a direct input to *compartment 0*, compare Fig. 4A. Consequently, the drop of the spiking probability is less sharp when the distal input arrives before the input at the spike initiation zone as compared to the drop on the right side of the maximum, Fig. 5D.

For injections even more distal there is no regime in which a spike could be triggered in all trials as the pulse is strongly attenuated when it reaches the spike initiation zone. The maximum probability of around 0.4 is reached at a delay of about −5 μs. For positive delays the spiking probability quickly decreases to zero; this decrease is again sharper than on the negative side of the maximum.

The membrane traces, Fig. 5B, show that an input to the most distal compartment has almost no effect on the membrane voltage of the compartment in which the dendritic spikes are generated. Consequently, the probability of triggering a spike stays low for all delays.

The probability of eliciting a dendritic spike can be increased by stronger synaptic inputs. Fig. 5E shows the probability of triggering a plateau potential for a fixed delay of −5 μs and different strengths of the additional input (the strength of the persistent input to *compartment 0* stays fixed). For all injection sites the spiking probability starts at zero for low weights and then transitions to one as the weight increases.

As EPSP are attenuated during their propagation along the chain, the transition is earlier and sharper the more proximal the additional input is to the spike initiation zone.

BAC induced burst firing

Layer 5 pyramidal neurons possess a sodium-spike as well as a calcium spike initiation zone (Larkum et al., 1999; Helmchen et al., 1999; Larkum, 2013). These zones allow the neuron to process the information arriving at the basal dendrites separately from the inputs to the tuft

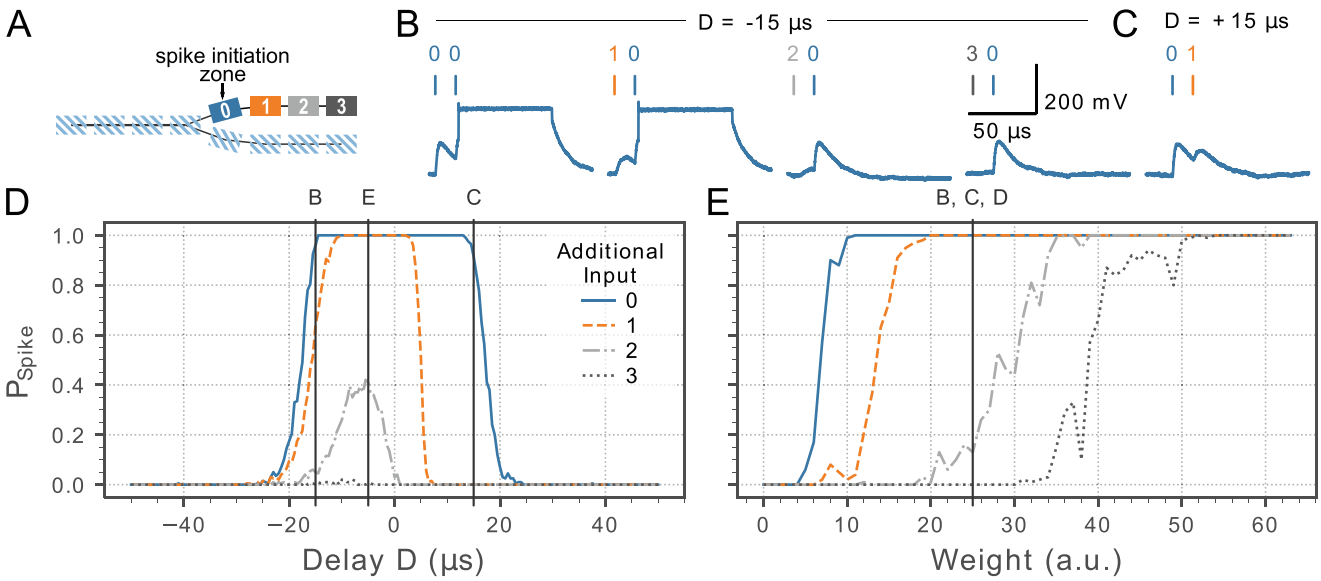

Fig. 5. Dendritic coincidence detection emulated on BSS-2. (**A**) A branching chain with four compartment in each branch is chosen to represent a thick dendrite which splits in two thinner dendrites. The first compartment of the upper thin branch (*compartment 0*) is configured to generate plateau potentials; all other compartments do not generate spikes. To test which distribution of spatio-temporal inputs trigger a spike, a synaptic input is always injected in *compartment 0* while an additional input is supplied to one further compartment with a delay *D*. (**B**) Example traces of the membrane voltage in *compartment 0* as an additional input is injected in different compartments with a delay of −15 µs. The vertical bars represent the time and site of synaptic input. The additional input is sufficient to trigger a dendritic plateau potential when injected in the first two compartments. More distal inputs can not trigger a spike at this delay. (**C**) Unlike for the negative delay in subfigure B, an input at *compartment 1* which precedes the input to *compartment 0* by 15 µs can not elicit a dendritic plateau potential. (**D**) Probability of eliciting a spike in *compartment 0* for different delays and different sites of the additional input. For each delay and injection site 200 experiments were performed. The time window in which a dendritic spike can be elicited with a high probability decreases the more distal the additional input is to the spike initiation site. Furthermore, distal inputs which are slightly before the proximal input are preferred for these sites. The vertical lines indicate delays which were used in the other subfigures. (**E**) Spiking probability for different strengths of the additional inputs. The delay was fixed to −5 µs and the probability was determined over 100 trials. The more proximal the site of the additional input the smaller the weight at which the spiking probability increases from zero. For all injection sites a dendritic spike could reliably be triggered if the weight was high enough. The vertical line marks the weight used in the other subfigures.

dendrites. In addition to the local integration, the two initiation zones can interact via the apical dendrite (Larkum et al., 1999; Larkum, 2013).

Sodium action potentials can travel to the calcium spike initiation zone and can facilitate the generation of calcium spikes. This is called back-propagating action potential activated calcium spike firing (BAC); the calcium spike propagates to the soma and can cause a burst of spikes. With this mechanism, information arriving at the two poles of the neuron can be linked.

This behavior can be replicated with a three-compartment model (Larkum et al., 2001), Fig. 6D, and was already demonstrated for prior versions of the BSS-2 system (Schemmel et al., 2017; Aamir et al., 2018a). It consists of a somatic compartment with sodium spike dynamics and a tuft compartment which can elicit Ca^{2+} spikes; both compartments are coupled via a passive compartment which represents the apical trunk.

As mentioned earlier, this model can be replicated on hardware with three neuron circuits, Fig. 3B. Again the different compartments are configured to have identical capacitances and comparable leak dynamics.

Synaptic input to the soma or distal part alone should not evoke burst firing. Fig. 6 shows that this is the case for our emulation on BSS-2. A synaptic input to the soma causes a single spike in the somatic compartment. The membrane potential rises due to the external stimulus and receives strong positive feedback upon crossing the exponential term's threshold V_{exp}, also compare sketch in Fig. 2. As soon as the threshold V_{th} is reached an output spike is generated and the membrane is connected to the reset potential V_{reset} for the duration of the refractory period τ_{ref}. The reset voltage V_{reset} was chosen to match the leak potential V_{leak}. As a consequence the refractory period is not clearly visible in the displayed membrane trace.

The other compartments follow the somatic membrane potential passively. As the pulse travels along the chain its maximum height decreases. In the chosen configuration the potential in the tuft compartment is not high enough to cause a plateau potential.

In contrast to input to the somatic compartment, the synaptic current injected in the distal part is not sufficient to trigger a spike in any compartment and the EPSP travels purely passively along the chain of compartments.

For coincident input the back-propagating sodium spike and the EPSP of the distal input sum up and trigger a plateau potential in the tuft compartment. Due to this plateau potential the potentials in the other compartments are increased. After the refractory period

of 10 μs the somatic membrane voltage increases quickly such that the soma ejects a burst of spikes until the plateau potential in the tuft compartment vanishes.

This example of BAC induced burst firing shows that the BSS-2 system is capable of emulating phenomena found in biological neurons.

DISCUSSION

The neuromorphic, mixed-signal BSS-2 system allows for the implementation of a large set of user-defined cell morphologies, Fig. 3, where the dynamics of neurons and synapses evolve accelerated with a speed-up of about 1000 compared to biological real-time."Linear" morphologies like three-compartment models or chains of compartments can be realized in a single row of neuron circuits. The second row of neuron circuits is available to construct more complex neuron morphologies.

A first experiment demonstrated the passive propagation of EPSP along a chain of compartments. As expected, synaptic inputs with the same strength cause a higher EPSP if the conductance between neighboring compartments is decreased. The attenuation of EPSP which travel along the chain can be controlled via the conductance between compartments.

Dendritic spikes come in different forms such as sodium spikes, calcium or NMDA plateau potentials. On the BSS-2 system sodium spikes can be modeled with the AdEx neuron model. NMDA and calcium potentials are replicated by plateau potentials, which can increase the membrane voltage for several tenth to hundredth of milliseconds (biological time).

The passive propagation in combination with dendritic spikes allows to implement a spatio-temporal coincidence detection in dendrites on BSS-2, Fig. 5. The spatial extent for which inputs are classified as coincident and therefore elicit a dendritic spike can for example be controlled by the synaptic weight, Fig. 5D. Utilizing the spatial dependency of this coincidence detection, direction selectivity could be implemented at the single neuron level (Tukker et al., 2004).

This new spatial component of the neuron allows to investigate phenomena like synaptic clustering. An algorithm similar to the one presented by Billaudelle et al. (2021) could be used to dynamically create and remove synapses on the dendritic tree (Poirazi and Mel, 2001; Hussain and Basu, 2016). A general purpose processor embedded on the BSS-2 chip has access to several state variables of the emulated, neural system and allows for the flexible implementation of learning rules (Friedmann et al., 2017).

The final experiment replicates the BAC induced burst firing found in pyramidal neurons, Fig. 6 (Larkum et al., 1999; Larkum et al., 2001). This mechanism relies on the bidirectional propagation of signals along the apical dendrite. On the BSS-2 neuromorphic chip signals can travel passively and bidirectionally between different compartments of a neuron and therefore allows for the replication of this mechanism.

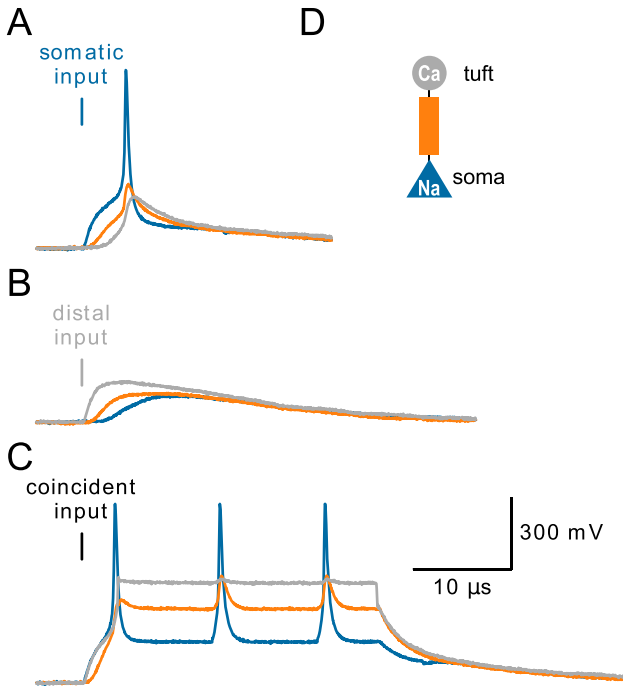

Fig. 6. Replication of BAC induced burst firing on BSS-2. (**A**) A synaptic input to the somatic compartment causes a sodium-like spike which propagates along the apical trunk towards the tuft compartment. Along the way the pulse gets attenuated and does not exceed the threshold for a dendritic plateau potential. (**B**) A single input to the tuft compartment is not sufficient to cause a dendritic plateau potential. (**C**) Both inputs combined cause a sodium-like spike response in the somatic compartment followed by a plateau potential in the tuft compartment. This in turn causes the soma to elicit two more spikes. (**D**) Three-compartment model proposed by Larkum et al. (2001) to replicate the BAC induced burst firing. A somatic compartment is via a passive compartment, which represents the apical trunk, connected to a tuft compartment. The somatic compartment can initiate sodium spikes while the tuft compartment elicits calcium plateau potentials.

In summary, the BSS-2 system is a highly configurable, mixed-signal, neuromorphic system which allows the accelerated emulation of networks of neurons with various morphologies. It supports both passive electric signals propagating through the compartments of these structured neurons as well as active dendritic spikes that can be initiated in the form of sodium-like spikes or plateau potentials. This gives researchers the opportunity to study the properties of neuromorphic implementations of spiking neuron networks beyond the point-neuron paradigm.

DECLARATION OF COMPETING INTEREST

The authors declare that they have no known competing financial interests or personal relationships that could have appeared to influence the work reported in this paper.

ACKNOWLEDGEMENTS

The authors wish to thank all present and former members of the Electronic Vision(s) research group

contributing to the BrainScaleS-2 experiment platform. This work has received funding from the EU ([FP7/2007–2013], [H2020/2014–2020]) under grant agreements 604102 (HBP), 720270 (HBP SGA1), 785907 (HBP SGA2) and 945539 (HBP SGA3) as well as from the Manfred Stärk Foundation.

REFERENCES

Aamir SA, Müller P, Kiene G, Kriener L, Stradmann Y, Grübl A, Schemmel J, Meier K (2018a) A mixed-signal structured AdEx neuron for accelerated neuromorphic cores. IEEE Trans. Biomed. Circuits Syst. 12(5):1027–1037. https://doi.org/10.1109/TBCAS.2018.2848203. ISSN 1932–4545.

Aamir S.A., Stradmann Y., Müller P., Pehle C., Hartel A., Grübl A., Schemmel J., Meier K., 2018. An Accelerated LIF Neuronal Network Array for a Large-Scale Mixed-Signal Neuromorphic Architecture. IEEE Trans. Circuits Syst. I: Regular Papers 65(12), 4299–4312. ISSN 1549–8328. doi:10.1109/TCSI.2018.2840718.

Agmon-Snir H, Carr C, Rinzel J (1998) The role of dendrites in auditory coincidence detection. Nature 393(6682):268–272.

Akar N.A., Cumming B., Karakasis V., Küsters A., Klijn W., Peyser A., Yates S., 2019. Arbor — a morphologically-detailed neural network simulation library for contemporary high-performance computing architectures. In: 2019 27th Euromicro International Conference on Parallel, Distributed and Network-Based Processing (PDP). pp. 274–282. doi:10.1109/EMPDP.2019.8671560.

Bhaduri A, Banerjee A, Roy S, Kar S, Basu A (2018) Spiking neural classifier with lumped dendritic nonlinearity and binary synapses: a current mode VLSI implementation and analysis. Neural Comput. 30:723–760. https://doi.org/10.1162/neco_a_01045. ISSN 1530–888X.

Billaudelle S., Stradmann Y., Schreiber K., Cramer B., Baumbach A., Dold D., Göltz J., Kungl A.F., Wunderlich T.C., Hartel A., Müller E., Breitwieser O., Mauch C., Kleider M., Grübl A., Stöckel D., Pehle C., Heimbrecht A., Spilger P., Kiene G., Karasenko V., Senn W., Petrovici M.A., Schemmel J., Meier K., 2020. Versatile emulation of spiking neural networks on an accelerated neuromorphic substrate. In: 2020 IEEE International Symposium on Circuits and Systems (ISCAS), IEEE. doi:10.1109/iscas45731.2020.9180741.

Billaudelle S, Cramer B, Petrovici MA, Schreiber K, Kappel D, Schemmel J, Meier K (2021) Structural plasticity on an accelerated analog neuromorphic hardware system. Neural Netw. 133:11–20. https://doi.org/10.1016/j.neunet.2020.09.024. ISSN 1879-2782.

Bono J, Wilmes KA, Clopath C (2017) Modelling plasticity in dendrites: from single cells to networks. Curr. Opin. Neurobiol. 46:136–141. https://doi.org/10.1016/j.conb.2017.08.013. ISSN 1873-6882.

Brette R, Gerstner W (2005) Adaptive Exponential Integrate-and-Fire Model as an Effective Description of Neuronal Activity. J. Neurophysiol. 94:3637–3642. https://doi.org/10.1152/jn.00686.2005.

Carnevale N.T., Hines M.L., 2006. The NEURON Book. Cambridge University Press, Cambridge, UK. ISBN 978-0521843218. doi:10.1017/CBO9780511541612.

Cramer B, Stöckel D, Kreft M, Wibral M, Schemmel J, Meier K, Priesemann V (2020) Control of criticality and computation in spiking neuromorphic networks with plasticity. Nat. Commun. 11:2853. https://doi.org/10.1038/s41467-020-16548-3. ISSN 2041–1723.

Cramer B., Billaudelle S., Kanya S., Leibfried A., Grübl A., Karasenko V., Pehle, C., Schreiber K., Stradmann Y., Weis J., Schemmel J., Zenke F. Training spiking multi-layer networks with surrogate gradients on an analog neuromorphic substrate, arXiv preprint.

Davison AP, Brüderle D, Eppler J, Kremkow J, Muller E, Pecevski D, Perrinet L, Yger P (2009) PyNN: a common interface for neuronal network simulators. Front. Neuroinform. 2(11). doi:3389/neuro.11.011.2008.

Euler T, Detwiler PB, Denk W (2002) Directionally selective calcium signals in dendrites of starburst amacrine cells. Nature 418:845–852. https://doi.org/10.1038/nature00931. ISSN 0028-0836.

Friedmann S, Schemmel J, Grübl A, Hartel A, Hock M, Meier K (2017) Demonstrating hybrid learning in a flexible neuromorphic hardware system. IEEE Trans. Biomed. Circuits Syst. 11 (1):128–142. https://doi.org/10.1109/TBCAS.2016.2579164. ISSN 1932–4545.

Golding NL, Spruston N (1998) Dendritic sodium spikes are variable triggers of axonal action potentials in hippocampal CA1 pyramidal neurons. Neuron 21:1189–1200. https://doi.org/10.1016/s0896-6273(00)80635-2. ISSN 0896-6273.

Golding NL, Staff NP, Spruston N (2002) Dendritic spikes as a mechanism for cooperative long-term potentiation. Nature 418:326–331. https://doi.org/10.1038/nature00854. ISSN 0028-0836.

Göltz J., Baumbach A., Billaudelle S., Breitwieser O., Dold D., Kriener L., Kungl A.F., Senn W., Schemmel J., Meier K., Petrovici M.A., 2019. Fast and deep neuromorphic learning with time-to-first-spike coding, arXiv preprint.

Guerguiev J, Lillicrap TP, Richards BA (2017) Towards deep learning with segregated dendrites. eLife 6. https://doi.org/10.7554/eLife.22901. ISSN 2050–084X.

Helmchen F, Svoboda K, Denk W, Tank DW (1999) In vivo dendritic calcium dynamics in deep-layer cortical pyramidal neurons. Nat. Neurosci. 2:989–996. https://doi.org/10.1038/14788. ISSN 1097-6256.

Hock M., Hartel A., Schemmel J., Meier K., 2013. An analog dynamic memory array for neuromorphic hardware. In: Circuit Theory and Design (ECCTD), 2013 European Conference on, 1–4, 2013. doi:10.1109/ECCTD.2013.6662229.

Hussain S, Basu A (2016) Morphological learning in multicompartment neuron model with binary synapses. In: Circuits and Systems (ISCAS), 2016 IEEE International Symposium on, IEEE. p. 2527–2530.

Koch C, Segev I (2000) The role of single neurons in information processing. Nat. Neurosci. 3:1171–1177. https://doi.org/10.1038/81444. ISSN 1097–6256.

Kousanakis E., Dollas A., Sotiriades E., Papaefstathiou I., Pnevmatikatos D.N., Papoutsi A., Petrantonakis P.C., Poirazi P., Chavlis S., Kastellakis G., 2017. An architecture for the acceleration of a hybrid leaky integrate and fire SNN on the convey HC-2ex FPGA-based processor. In: 2017 IEEE 25th Annual International Symposium on Field-Programmable Custom Computing Machines (FCCM), IEEE. doi:10.1109/fccm.2017.51.

Larkum M (2013) A cellular mechanism for cortical associations: an organizing principle for the cerebral cortex. Trends Neurosci. 36 (3):141–151.

Larkum ME, Zhu JJ, Sakmann B (1999) A new cellular mechanism for coupling inputs arriving at different cortical layers. Nature 398:338–341. https://doi.org/10.1038/18686. ISSN 0028-0836.

Larkum ME, Zhu JJ, Sakmann B (2001) Dendritic mechanisms underlying the coupling of the dendritic with the axonal action potential initiation zone of adult rat layer 5 pyramidal neurons. J. Physiol. 533(2):447–466. https://doi.org/10.1111/j.1469-7793.2001.0447a.x. ISSN 0022–3751.

Larkum, M.E., Senn, W., Lüscher, H.-R., 2004. Top-down dendritic input increases the gain of layer 5 pyramidal neurons. Cerebral Cortex 14(10), 1059–1070. ISSN 1047–3211. doi:10.1093/cercor/bhh065.

Larkum ME, Nevian T, Sandler M, Polsky A, Schiller J (2009) Synaptic integration in tuft dendrites of layer 5 pyramidal neurons: a new unifying principle. Science 325(5941):756–760.

London M, Häusser M (2005) Dendritic computation. Annu. Rev. Neurosci. 28:503–532.

Major G, Larkum ME, Schiller J (2013) Active properties of neocortical pyramidal neuron dendrites. Annu. Rev. Neurosci.

36:1–24. https://doi.org/10.1146/annurev-neuro-062111-150343. ISSN 1545–4126.

Müller E., Mauch C., Spilger P., Breitwieser O.J., Klähn J., Stöckel D., Wunderlich T., Schemmel J. Extending BrainScaleS OS for BrainScaleS-2, arXiv preprint.

Poirazi P, Mel BW (2001) Impact of active dendrites and structural plasticity on the memory capacity of neural tissue. Neuron 29:779–796. https://doi.org/10.1016/s0896-6273(01)00252-5. ISSN 0896-6273.

Poirazi P, Brannon T, Mel BW (2003) Pyramidal neuron as two-layer neural network. Neuron 37:989–999. https://doi.org/10.1016/s0896-6273(03)00149-1. ISSN 0896-6273.

Polsky A, Mel BW, Schiller J (2004) Computational subunits in thin dendrites of pyramidal cells. Nat. Neurosci. 7:621–627. https://doi.org/10.1038/nn1253. ISSN 1097-6256.

Rall W (1959) Branching dendritic trees and motoneuron membrane resistivity. Exp. Neurol. 1(5):491–527.

Ramakrishnan S, Wunderlich R, Hasler J, George S (2013) Neuron array with plastic synapses and programmable dendrites. IEEE Trans. Biomed. Circuits Syst. 7:631–642. https://doi.org/10.1109/TBCAS.2013.2282616. ISSN 1940-9990.

Richards BA, Lillicrap TP (2019) Dendritic solutions to the credit assignment problem. Curr. Opin. Neurobiol. 54:28–36. https://doi.org/10.1016/j.conb.2018.08.003. ISSN 1873-6882.

Sacramento, J., Costa, R.P., Bengio, Y., Senn, W. Dendritic cortical microcircuits approximate the backpropagation algorithm, arXiv preprint.

Schaefer AT, Larkum ME, Sakmann B, Roth A (2003) Coincidence detection in pyramidal neurons is tuned by their dendritic branching pattern. J. Neurophysiol. 89:3143–3154. https://doi.org/10.1152/jn.00046.2003. ISSN 0022-3077.

Schemmel, J., Kriener, L., Müller, P., Meier, K., 2017. An accelerated analog neuromorphic hardware system emulating nmda- and calcium-based non-linear dendrites. In: 2017 International Joint Conference on Neural Networks (IJCNN), 2217–2226. doi:10.1109/IJCNN.2017.7966124.

Schemmel, J., Billaudelle, S., Dauer, P., Weis, J. Accelerated Analog Neuromorphic Computing, arXiv preprint.

Schiller J, Major G, Koester HJ, Schiller Y (2000) NMDA spikes in basal dendrites of cortical pyramidal neurons. Nature 404 (6775):285–289.

Stimberg M, Brette R, Goodman DF (2019) Brian 2, an intuitive and efficient neural simulator. eLife 8. https://doi.org/10.7554/eLife.47314.

Tukker JJ, Taylor WR, Smith RG (2004) Direction selectivity in a model of the starburst amacrine cell. Visual Neurosci. 21:611–625. https://doi.org/10.1017/S0952523804214109. ISSN 0952-5238.

Ujfalussy BB, Makara JK, Lengyel M, Branco T (2018) Global and multiplexed dendritic computations under in vivo-like conditions. Neuron 100. https://doi.org/10.1016/j.neuron.2018.08.032. 579–592.e5, ISSN 1097–4199.

Urbanczik R, Senn W (2014) Learning by the dendritic prediction of somatic spiking. Neuron 81(3):521–528. https://doi.org/10.1016/j.neuron.2013.11.030. ISSN 1097–4199.

Vetter P, Roth A, Häusser M (2001) Propagation of action potentials in dendrites depends on dendritic morphology. J. Neurophysiol. 85:926–937. https://doi.org/10.1152/jn.2001.85.2.926. ISSN 0022-3077.

Wang Y, Liu S-C (2011) A two-dimensional configurable active silicon dendritic neuron array, circuits and systems I: regular papers. IEEE Trans. 58(9):2159–2171. https://doi.org/10.1109/TCSI.2011.2112570. ISSN 1549–8328.

Williams SR, Stuart GJ (2002) Dependence of EPSP efficacy on synapse location in neocortical pyramidal neurons. Science 295:1907–1910. https://doi.org/10.1126/science.1067903. ISSN 1095-9203.

Yi G, Wang J, Wei X, Deng B (2017) Action potential initiation in a two-compartment model of pyramidal neuron mediated by dendritic Ca^{2+} spike. Scientific Rep. 7:45684. https://doi.org/10.1038/srep45684. ISSN 2045-2322.

(Received 9 March 2021, Accepted 11 August 2021)
(Available online xxxx)